Ionospheric E-Region Response to Solar-Geomagnetic Storms Observed by TIMED/SABER and Application to IRI Storm-Model Development

Christopher J. Mertens[a,*], Jeffrey C. Mast[b], Jeremy R. Winick[c], James M. Russell III[d], Martin G. Mlynczak[a], and David S. Evans[e]

[a,*] *NASA Langley Research Center, Hampton, VA 23681-2199, United States*
[b] *SAIC Inc, Hampton, VA 23666, United States*
[c] *Air Force Research Laboratories, Hanscom AFB, MA 01731-3010, United States*
[d] *Center for Atmospheric Sciences, Hampton University, Hampton VA 23668, United States*
[e] *NOAA Space Environment Center, Boulder CO 80303, United States*
[*] *Corresponding author. Tel.: +1 757 864 2179; Fax: +1 757 864 6326. Email address: c.j.mertens@larc.nasa.gov (C. J. Mertens)*

Abstract

The large thermospheric infrared radiance enhancements observed from the TIMED/SABER experiment during recent solar storms provide an exciting opportunity to study the influence of solar-geomagnetic disturbances on the upper atmosphere and ionosphere. In particular, nighttime enhancements of 4.3 um emission, due to vibrational excitation and radiative emission by NO^+, provide an excellent proxy to study and analyze the response of the ionospheric E-region to auroral electron dosing and storm-time enhancements to the E-region electron density. In this paper we give a status report of on-going work on model and data analysis methodologies of deriving NO^+ 4.3 um volume emission rates, a proxy for the storm-time E-region response, and the approach for deriving an empirical storm-time correction to IRI E-region NO^+ and electron densities.

1. Introduction

The Sounding of the Atmosphere using Broadband Emission Radiometry (SABER) instrument is a broadband infrared limb sounder on the Thermosphere-Ionosphere-Mesosphere-Energetics and Dynamics (TIMED) satellite (Russell et al., 1999). TIMED was launched in 2001 and has observed the atmospheric response to several major solar eruptive events. The two events considered in this paper are the April 2002 and the `Halloween' (October-November) 2003 solar storms. Large enhancements of thermospheric infrared emission were observed by several of the SABER radiometer channels during these storm periods (Mlynczak et al., 2003, 2005; Mertens et al., 2005). Specific to this paper, several orders of magnitude enhancement in the nighttime SABER 4.3 um limb emission measurements were observed due to storm-time excitation of the vibration-rotation bands of NO^+ (Mertens et al., 2005). During solar-geomagnetic storms, electron precipitation increases the ionization of the neutral atmosphere producing primarily N_2^+, O_2^+, O^+, and N^+ (e.g., Banks et al., 1974; Strickland et al., 1976). In the E-region, these ions react with the neutral species to produce NO^+ (Torr et al., 1990; Fox and Sung, 2001). Some of the ion-neutral reactions are exothermic enough to produce

vibrationally excited NO^+, i.e., $NO^+(v)$, which emits at 4.3 um (Winick et al., 1987b). The exothermic reactions are relatively fast. Above ~ 110 km quenching of $NO^+(v)$ becomes less important and prompt emission of $NO^+(v)$ at 4.3 um is a direct measure of auroral dosing in the E-region. Since NO^+ is the terminal E-region ion, the SABER 4.3 um measurements are a useful dataset for analyzing the E-region response to solar-geomagnetic storms. Moreover, because of charge neutrality, enhancements in 4.3 um emission are indicative of enhancements in both the NO^+ and electron densities.

The derived quantity used to analyze the E-region response to solar-geomagnetic activity from the SABER measurements is $NO^+(v)$ 4.3 um volume emission rates (VER). The $NO^+(v)$ fundamental band (2344 cm^{-1}) is nearly coincident with the strong major isotopic $CO_2(\nu_3)$ band at 2349 cm^{-1}. Therefore, $NO^+(v)$ VER is derived from SABER 4.3 um limb emission measurements by (1) removing the background contributions of $CO_2(\nu_3)$ emission from the measured 4.3 um limb radiance, and (2) performing a standard Abel inversion on the residual radiance to obtain vertical profiles of $NO^+(v)$ VER. The $CO_2(\nu_3)$ 4.3 um contribution can be removed to within ~ 20% using SABER data products and the SABER non-LTE CO_2 model and radiation transfer algorithms (see section 4) during quiescent conditions, consistent with the findings of Lopez-Puertas et al. (2004). Under strong storm conditions, however, there is the possibility of significant auroral energy deposition into $N_2(v)$, which couples to $CO_2(\nu_3)$ through equation (5), which may potentially complicate the ability to remove $CO_2(\nu_3)$, with the result of an increase in the uncertainty in removing the background $CO_2(\nu_3)$ contribution. This topic is discussed further in section 4.

The ionospheric E-region parameters are largely inaccessible to observation, especially on a global scale. Therefore, SABER measurements provide a novel dataset for analyzing the E-region. We anticipate that the $CO_2(\nu_3)$ contributions to the SABER 4.3 um limb emission measurements can be removed to within reasonable accuracy (i.e., ~20%), especially since the observational and theoretical evidence suggests that $NO^+(v)$ 4.3 um emission dominates the overall 4.3 um emission during strong storms (see sections 2 and 3). Consequently, the $NO^+(v)$ VER is an excellent proxy for studying the E-region under disturbed conditions. The advantages of the SABER data are: (1) the data are global measurements, with observations made over the entire duration of recent major solar storms; (2) SABER measurements and the derived data products have a high vertical resolution (~ 2 km); and (3) the derived $NO^+(v)$ VER is independent of an assumed profile shape and potentially independent of any chemical, kinetic, or spectroscopic rate coefficients (see section 4).

Efforts are currently underway to use the $NO^+(v)$ VER to assess current understanding of fundamental E-region energy transfer mechanisms from auroral energy deposition, to ion-neutral reactions, to radiative loss. Because of the paucity of infrared auroral emission observations and laboratory measurements, there are still large uncertainties in these fundamental E-region ion-neutral processes (Mertens et al., 2005). However, in this paper we concentrate on an application that is independent of our understanding of E-region chemistry and energetics. Because of point number (3) listed above, the SABER-

derived $NO^+(v)$ VER is a suitable proxy for deriving an empirical storm-time correction to the International Reference Ionosphere (IRI) E-region NO^+ and electron densities.

The IRI is a widely used empirical model for the specification of ionospheric parameters and is recommended for international use by the Committee On Space Research (COSPAR) and the International Union of Radio Science (URSI) (Bilitza, 2001). An important functionality of the IRI model needed for space-weather-related applications is the accurate characterization of ionospheric parameters during solar-geomagnetic storms. The goal of developing algorithms for updating IRI parameters during storm-time conditions remains a high priority of the IRI team. However, knowledge of the ionospheric response to solar-geomagnetic disturbances remains largely incomplete and the recent release of IRI-2000 (Bilitza, 2001) is the first version of IRI to include any geomagnetic activity dependence, but only for the F-region densities. The STORM model developed by Araujo-Pradere et al. (2002, 2003) is a first step toward capturing the underlying ionospheric F-region response in a simple empirical model.

Currently there is no storm-time correction to IRI parameters in the E-region. SABER observations suggest several orders of magnitude in the E-region dominant ion (i.e., NO^+) and electron densities during the April 2002 and Halloween 2003 solar storms (see section 2). An error of several orders of magnitude in the IRI E-region parameterization will limit the model's usability in radio wave propagation models – as applied to system design of communication, navigation, and surveillance systems – and real-time processing of the radio wave propagation data during solar-geomagnetic storms. Errors in E-region electron density of several orders of magnitude can induce non-negligible errors in modeling vertical and slant path radio wave propagation (satellite to ground communication). Moreover, significant errors can be induced in modeling satellite to satellite radio wave propagation along long horizontal paths. To improve the utility and range of applicability of the IRI model, we have initiated a plan to develop an empirical storm-time correction to the IRI E-region NO^+ and electron densities using infrared emission measurements from the TIMED/SABER instrument.

The purpose of this paper is to (1) demonstrate the efficacy of $NO^+(v)$ VER as a proxy for the E-region response to solar-geomagnetic storms, (2) describe the derivation of $NO^+(v)$ VER from SABER 4.3 um limb emission measurements, and (3) outline an approach to derive an empirical storm-time correction to IRI E-region NO^+ and electron densities.

2. Observational basis for E-region proxy

During the daytime, radiative emission by CO_2 dominates the 4.3 um spectral region due to solar pumping of the $CO_2(\nu_1,\nu_2,\nu_3)$ vibration-rotation bands. During strong nighttime aurora, on the other hand, 4.3 um emission is dominated by contributions from $NO^+(v)$ vibration-rotation bands (Winick et al., 1987a, 2004). Therefore, we utilize nighttime SABER 4.3 um emission measurements to derive $NO^+(v)$ VER as our proxy to characterize the E-region response to solar-geomagnetic disturbances. In this section we

present observational rationale for using $NO^+(v)$ VER, derived from SABER 4.3 um limb radiance measurements, as our E-region proxy.

Emission by $NO^+(v)$ in the 4.3 um spectral region was first identified by Picard et al. (1987) and Espy et al. (1988), and later by others (e.g., Caledonia et al., 1995; Dothe et al., 1996; and Smith et al., 2000). More recently, SABER observed several orders of magnitude enhancements of nighttime 4.3 um emission during strong aurora. Figure 1 shows representative profiles measured by the SABER (channel 7) 4.3 um radiometer channel during the April 2002 and Halloween 2003 solar storms. The vertical, dashed line in the figure is the channel-7 noise equivalent radiance (NER), which is 7.35×10^{-7} W m^{-2} sr^{-1}. Prior to the onset of the storm periods, the radiance decreases with increasing altitude reaching the detector noise level by ~ 135 km. During the peak of the solar storms, the 4.3 um radiance is enhanced by up to several orders of magnitude and doesn't reach the detector noise limit until above 180 km. As a result, we take the upper boundary of our analysis region to be 180 km.

Figure 2 shows daily-averaged NOAA/POES and SABER measurements for representative days during the April 2002 and Halloween 2003 solar storms. The left-hand column is in-situ measurements of total electron energy flux made by the National Oceanic and Atmospheric Administration (NOAA) low energy Total Energy Detector (TED)and Medium Energy Proton and Electron Detector (MEPED) instruments on board the Polar Orbiting Environmental Satellites (POES). The right-hand column is SABER 4.3 um channel measurements of limb emission at 140 km, in units of NER. SABER was observing in the southern hemisphere polar region during the April 2002 storm. The first row in Figure 2 is the southern hemisphere data from 60S to 84N. During the Halloween 2003 storm, SABER was sampling in the northern hemisphere polar region. The second row in Figure 2 is the northern hemisphere data from 60N to 84N. The SABER data in Figure 2 are averaged nighttime measurements (nighttime profiles defined by a solar zenith angle greater than 104 degrees) where as the POES data are averaged daytime and nighttime measurements.

The Halloween 2003 storm was a substantially larger storm event compared to the April 2002 storm. In Figure 2, the maximum single-event electron flux measurement on 20 April was 29 ergs/cm^2/s at 62S, 73E, 15:36:09 UT with a characteristic energy of 6.7 keV. The maximum daily-average for 20 April was 8.4 ergs/cm^2/s at 74S, 36E with a characteristic energy of 9.8 keV. Likewise, the maximum single-profile 4.3 um radiance measurement at 140 km on 20 April was 42 (NER units) at 60S, 211E, 05:05:43 UT. The maximum daily-average was 37 (NER units) at 61S, 46E on 20 April. On 30 October the largest single-event electron flux measured was 27 ergs/cm^2/s at 73N, 112E, 20:34:38 UT with a characteristic energy of 2.6 keV. The maximum daily-average electron flux was 18 ergs/cm^2/s with a characteristic energy of 524 eV at 76N, 46E on 30 October. Moreover, the maximum single-profile 4.3 um radiance measurement at 140 km on 30 October was 117 (NER units) at 64N, 104E, 19:28:45 UT, while the 30 October maximum daily-average was 110 (NER units) at 64N, 104E. These data will be used in simulations in section 3.

Figure 2 clearly shows the spatial correlations between auroral electron dosing and 4.3 um emission, especially for the April 2002 storm. Although regions of high/low electron dosing for October 30, 2003 generally correspond to regions of large/small enhancements in the 4.3 um emission, the 4.3 um data is much more complicated with large enhancements outside the regions of strong auroral dosing, as indicated by the NOAA/POES data. A full understanding of the differences between the two storms, as evident in Figure 2, requires analysis of additional datasets combined with physics-based model simulations, which we plan to do in a future report. Broadly speaking, however, we expect that differences in ionization rates, as indicated by the different average characteristic energies between the two storms, will have a significant effect. A low characteristic energy of order ~ 1 keV, typical of the Halloween storm, will produce an ionization rate profile with a broad vertical peak and relatively large contributions from the high altitude tail (~ 130 km and greater). Thus, a precipitating electron energy distribution with a low characteristic energy requires much less total energy flux to produce the same ionization rate at 140 km, for example, than an energy distribution with a larger characteristic energy (say ~ 6-9 keV, typical of the April 2002 storm). The regions of low total energy flux on October 30, 2006, as shown in Figure 2, may actually have significant ionization at high altitudes such as the 140 km altitude level shown for the SABER 4.3 um emission. As a result, the 4.3 um emission appears to fill in the gaps, so to speak, between the regions of high precipitating total electron energy flux for the Halloween 2003 storm. Differences in the thermal structure, composition, and transport between the two storm periods will undoubtedly play a role as well in understanding the difference in 4.3 um radiative response to auroral dosing, via the reactions (1)-(4).

In short, the comparisons between electron precipitation and 4.3 um emission shown in Figure 2 demonstrate that thermospheric infrared emission at 4.3 um is a suitable proxy for observing the ionospheric E-region response to solar-geomagnetic forcing. Fortunately, the storm-time correction to the E-region NO^+ and electron densities, the topic of this paper, is based on a statistical data fit and requires no quantitative understanding of the complex physical mechanisms that give rise to the enhancements in the 4.3 um emission.

3. Theoretical basis for E-region proxy

In this section we present the theoretical rationale for using $NO^+(v)$ VER as our E-region proxy. The ion-neutral reactions that are sufficiently exothermic to produce vibrationally excited NO^+ in the E-region are as follows (Winick et al., 1987b; Caledonia et al., 1995; Dothe et al., 1996; and Smith et al., 2000):

$$\begin{aligned} N_2^+ + O &\rightarrow NO^+(v) + N(^4S) + 3.08eV \quad (v_{\max} = 10) \\ &\rightarrow NO^+(v) + N(^2D) + 0.69eV \quad (v_{\max} = 2) \end{aligned} \qquad \textbf{(1)}$$

$$\begin{aligned} N^+ + O_2 &\rightarrow NO^+(v) + O(^1S) + 2.43eV \quad (v_{\max} = 8) \\ &\rightarrow NO^+(v) + O(^1D) + 4.66eV \quad (v_{\max} = 18) \\ &\rightarrow NO^+(v) + O(^3P) + 6.63eV \quad (v_{\max} = 28) \end{aligned} \tag{2}$$

$$O^+ + N_2 \rightarrow NO^+(v) + N(^4S) + 1.1eV \quad (v_{\max} = 3) \tag{3}$$

$$\begin{aligned} O_2^+ + NO &\rightarrow NO^+(v) + O_2(X) + 2.83eV \quad (v_{\max} = 9) \\ &\rightarrow NO^+(v) + O_2(a) + 1.85eV \quad (v_{\max} = 6) \\ &\rightarrow NO^+(v) + O_2(b) + 1.20eV \quad (v_{\max} = 4) \end{aligned} \tag{4}$$

Reaction (1) dominates the production of $NO^+(v)$ and subsequent 4.3 um emission above 140 km (Winick et al., 1987b; Caledonia et al., 1995; Dothe et al., 1996; and Smith et al., 2000). Below 140 km, reaction (2) is an important contributor (Winick et al., 1987b; Caledonia et al., 1995). Significant contributions from reaction (3) occur at altitudes above ~ 160 km (Smith et al., 2000; Duff and Smith, 2000). The large exothermicity of reaction (4) makes the production of $NO^+(v)$ possible. This process would be important for high [NO], which occurred during recent solar-geomagnetic storms [Richards, 2004; Mlynczak et al., 2003, 2005]. However, there has been no evidence to date of vibrational excitation of NO^+ from this reaction. Furthermore, it is believed, based on reaction kinetics, that vibrational excitation of the product is less likely for charge transfer reactions where no new bond is formed [Winick et al., 1987b]. As a result, we neglect this reaction in this paper, although we will consider this reaction in future work as a possible mechanism, via transport of [NO] out of the auroral dosing region, which may be responsible for the mid-latitude enhancements of 4.3 um emission shown in Figure 2 for 30 October, 2003.

Reactions (1)-(3) are the chemical mechanisms considered in the subsequent analysis which produce vibrationally excited NO^+. The important loss mechanisms of $NO^+(v)$ are collisional quenching and radiative loss. Quenching of $NO^+(v)$ above 130 km is negligible, but becomes an important mechanism below 110 km (Winick et al., 1987b). The fundamental and hot 4.3 um transitions ($\Delta v = 1$) are the dominant radiative loss processes (Werner and Rosmus, 1982).

We computed the reactants of (1)-(3) with the field-line interhemispheric plasma (FLIP) model (Richards, 2002). Figure 3 shows FLIP simulations of the ion and neutral densities in (1)-(3) for a quiet and disturbed day during the April 2002 solar storm period. The auroral dosing for the disturbed day is 9 ergs/cm^2/s with a characteristic energy of 6 keV. The input auroral dosing to FLIP is consistent with the maximum daily-averaged auroral dosing measured by POES for 20 April, 2002 (see previous section). Note the difference in horizontal scales for the ion densities in Figure 3. The NO^+ density (and the electron density by charge neutrality) is approximately two orders of magnitude greater during the

disturbed day compared to the quiet day, which is similar to the SABER-observed enhancement in 4.3 um emission shown in Figure 1.

The 4.3 um limb emission from $NO^+(v)$ can be computed from known chemical, kinetic, and spectroscopic parameters using infrared radiation transfer algorithms (Mertens et al., 1999, 2002). The steady-state $NO^+(v)$ densities are calculated from the production processes in (1)-(3) and vibrational loss mechanisms described above (Winick et al., 1987b; Caledonia et al., 1995; Dothe et al., 1996; Smith et al., 2000). The 4.3 um limb radiance is calculated using the steady-state $NO^+(v)$ densities and absorption line parameters from the HITRAN 2000 molecular spectroscopic database (Rothman et al., 2003). Figure 4 shows the simulated April 2002 4.3 um limb spectra for the same quiet day and disturbed day as presented in the simulations shown in Figure 3. It's evident from Figure 4 that $NO^+(v)$ dominates the E-region limb emission, both over the entire 4.3 um spectral region and within the SABER 4.3 um channel spectral bandpass.

In sections 2 and 3 we have presented the observational and theoretical rationale for choosing $NO^+(v)$ VER as a proxy for characterizing the E-region response to solar-geomagnetic disturbances. In sections 4 and 5 we present the method of deriving $NO^+(v)$ VER from the SABER 4.3 um limb emission measurements.

4. Removal of $CO_2(\nu_3)$ 4.3 um background emission

The first step in deriving $NO^+(v)$ VER is subtracting the background $CO_2(\nu_3)$ emission from the measured 4.3 um limb radiance. This can be done with the radiation transfer algorithms used in the operational processing of the SABER data. The $CO_2(\nu_3)$ contribution is removed using the 4.3 um forward radiance component of the operational non-local thermodynamic equilibrium (non-LTE) kinetic temperature (Tk) and CO_2 volume mixing ratio (vmr) retrieval algorithm (Mertens et al., 2002, 2005). The forward model is comprised of two parts: (1) the CO_2 vibrational temperature (Tv) model and (2) the limb radiance model. Limb radiance is calculated using BANDPAK (Marshall et al., 1994), which is based on emissivity databases calculated line-by-line using LINEPAK routines (Gordley et al., 1994). The CO_2 Tv model is based on the Modified Curtis Matrix approach (Lopez-Puertas et al., 1986a-b, 1998), and uses BANDPAK in all the radiation transfer calculations. The SABER operational forward model used in this analysis is in excellent agreement with industry standards for infrared radiative transfer modeling (Mertens et al., 1999; Edwards et al., 1993; Lopez-Puertas et al., 1998; and Wintersteiner et al., 1992).

The nighttime $CO_2(\nu_3)$ contribution to the SABER-measured 4.3 um limb emission is simulated with the non-LTE radiation transfer algorithms described above using input atmospheric data from SABER-retrieved Tk and pressure, CO_2 vmr from a TIME-GCM climatological database (Roble et al., 1995), and composition data (N_2, O_2, O) from the NRLMSIS-00 model (Picone et al., 2002). All input composition data (CO_2, N_2, O_2, O) to the CO_2 Tv model for the nighttime 4.3 um limb radiance calculations are consistent with the operational processing of SABER data below 120 km. Above 120 km Tk and

composition are obtained from the NRLMSIS-00 model (CO_2 still comes from the TIME-GCM database). Pressure is extended above 120 km assuming hydrostatic equilibrium.

The OH(v) VER data product from the SABER 2.0 um channel measurement is used to calculate the vibrational excitation of $N_2(1)$ from collisions of ground state N_2 with OH($v \leq 9$). The method of calculating the total production rate of OH(v) from measured OH(v) VER at 2.0 um is by Mlynczak et al. (1998), while the method of calculating the rate of production of $N_2(1)$ from OH(v) is by Lopez-Puertas et al. (2004). Energy transfer from vibrationally excited OH (i.e., OH($v \leq 9$)) to $N_2(1)$, and then to $CO_2(\nu_3)$ via the V-V transfer mechanism in (5), is an important source of nighttime CO_2 4.3 um emission starting from 70 km and extending to above 120 km (Lopez-Puertas et al., 2004). The influence of this excitation process extends well above the OH layer due to the non-LTE process of local excitation (OH($v \leq 9$) → $N_2(1)$ → $CO_2(\nu_3)$) followed by radiative loss and re-absorption at higher altitudes. Once the nighttime $CO_2(\nu_3)$ 4.3 um limb radiance is calculated, it is subtracted from the SABER 4.3 um radiance measurement. The residual radiance is emission from $NO^+(v)$. The $NO^+(v)$ VER is derived by performing an Abel inversion on the residual radiance (section 5).

The SABER Tk and pressure in the mesosphere and lower thermosphere (MLT) are retrieved from (channel-1) CO_2 15 um limb emission measurements. The signal-to-noise ratio in the 15 um limb radiance measurements approaches unity at approximately ~ 130 km (Mertens et al., 2001). The theoretical limit to the MLT Tk and pressure retrieval, based on the available noise-free information content in the radiance measurement, is roughly 120 km (Mertens et al., 2002). However, the uncertainty in retrieved Tk and pressure increases significantly above 100 km due to increasing measurement noise, uncertainty in the atomic oxygen concentration, and the rate of quenching of $CO_2(\nu_2)$ by atomic oxygen (Mertens et al., 2001, 2004).

The demonstrated accuracy of the SABER temperatures and pressures below 100 km gives confidence in the ability to model the CO_2 non-LTE processes and the infrared radiation transfer, in general (Mertens et al., 2004). The large uncertainty in the SABER Tk and pressure above 100 km, and the uncertainty associated with using the NRLMSIS-00 model above 120 km, however, should have a small overall effect on the retrieved $NO^+(v)$ VER. The CO_2 Tv's needed to model the nighttime 4.3 um emission approach their radiative equilibrium values above 100 km, which is a balance between radiative pumping from lower altitudes and radiative loss at 4.3 um (Lopez-Puertas et al., 1986b). Thus, the CO_2 Tv's above 100 km depend mostly on the thermal structure and composition below 100 km, which is accurately known from the SABER Tk and pressure retrievals and the composition data from the TIME-GCM and NRLMSIS-00 models, with small dependence on the local CO_2 density between ~ 100-140 km. The uncertainties in removing the $CO_2(\nu_3)$ contribution mainly effects the quiescent $NO^+(v)$ VER retrieval since $NO^+(v)$ dominates the 4.3 um radiative emission during solar-geomagnetic storms, which will tend to overshadow the uncertainties in modeling the $CO_2(\nu_3)$ emission.

Figure 5 shows the contribution due to $CO_2(\nu_3)$ and $NO^+(v)$ in the SABER 4.3 um limb radiance channel under low geomagnetic activity and for high geomagnetic activity – i.e.,

with the daily-averaged auroral dosing characteristic of 20 April, 2002. Under quiescent to low geomagnetic activity conditions, the $CO_2(\nu_3)$ contribution is largely 100% of the total 4.3 um limb emission . Under strong storm conditions, the $CO_2(\nu_3)$ contribution is generally less than 20% of the total 4.3 um limb emission with a maximum of 40% at 130 km. The error in the simulated nighttime 4.3 um limb radiance is expected to be less than 20% (Lopez-Puertas et al., 2004). Our simulations are consistent with this finding. Thus, the simulation of $CO_2(\nu_3)$ 4.3 um limb radiance will introduce no more than a 4-8% error in the derived $NO^+(v)$ contribution to the measured 4.3 um limb emission under strong storm conditions.

Because the exothermic reactions (1)-(3) are fast and collisional quenching is rare above 110 km, emission of $NO^+(v)$ at 4.3 um is prompt and a direct indication of auroral dosing in the E-region (Winick et al., 1987a). Below 110 km, quenching of $NO^+(v)$ becomes increasingly important and near-resonant vibration-vibration (V-V) transfer between $CO_2(\nu_3)$ and $N_2(v)$ introduces a chemical time constant through auroral energy deposition into $N_2(v)$, which is transferred to $CO_2(\nu_3)$ via reaction (5) (Winick et al., 1987a).

$$CO_2(\nu_3) \quad + \quad N_2(v) \quad \leftrightarrow \quad CO_2(\nu_3 - 1) \quad + \quad N_2(v+1) \quad + \quad 18cm^{-1} \tag{5}$$

Auroral electrons vibrationally excite molecular nitrogen through inelastic collisions between low energy secondary electrons and N_2 (Newton et al., 1974) and chemical reactions (Richards et al., 2002). The auroral excitation of $N_2(v)$ affects the local $CO_2(\nu_3)$ 4.3 um emission through the V-V exchange in (5). Above 110 km, $N_2(v)$ is quenched by collisions with atomic oxygen and locally decouples from $CO_2(\nu_3)$. However, aurora can influence $CO_2(\nu_3)$ 4.3 um emission above 110 km through non-LTE processes due to V-V exchange between $CO_2(\nu_3)$ and $N_2(v)$ below 110 km followed by radiative transport to higher altitudes. Thus, the coupling mechanism in reaction (5) may complicate the ability to remove $CO_2(\nu_3)$ under strong auroral dosing since little is known about the effects of this mechanism both theoretically and observationally. We anticipate that the spectrally-resolved observations provided by the MIPAS instrument on Envisat during the January 2005 solar storm will contribute to quantifying the partitioning of $CO_2(\nu_3)$ and $NO^+(v)$ 4.3 um emission under strong storm conditions. The chemical lifetime is further complicated below ~ 90 km by radiative trapping in the $CO_2(\nu_3)$ vibration-rotation bands and transfer of quanta back to $N_2(v)$. Consequently, the lower boundary of our analysis region is 90 km.

5. E-region proxy: SABER-derived $NO^+(v)$ VER

The second step in deriving the $NO^+(v)$ VER is to perform an Abel inversion on the observed residual radiance (measured 4.3 um radiance minus $CO_2(\nu_3)$ contribution), which is the contribution to the SABER-measured 4.3 um emission due to $NO^+(v)$. $NO^+(v)$ 4.3 um radiative transfer is optically thin at all altitudes (Winick et al., 1987a-b). Thus, the observed residual radiance can be described by the weak-line form of the radiation transfer equation. By transforming the spatial coordinate from the horizontal

path along the limb line-of-sight to vertical distance, the measured residual radiance is represented by the following integral equation

$$2\pi \Delta L(z_t) = \int_{R(z_t)}^{R(\infty)} K(R)V(R)dR \tag{6}$$

where $\Delta L(z_t)$ is the residual radiance at tangent height z_t, K(R) is the kernel of the integral equation as a function of radial distance from earth-center (R), V(R) is the volume emission rate, and $R(z_t)$ is the radial distance at tangent height z_t. The kernel depends only on geometric factors.

$$K(R) = \frac{R(z)}{\sqrt{R^2(z) - R^2(z_t)}} \tag{7}$$

The integral equation in (6) with a kernel of the form (7) is known as an Abel Integral Equation [Arfken, 1985]. Solving for the unknown on the right-hand-side of (6), i.e., V(R), is called an Abel inversion. Regardless of the specific form of the kernel, (6) is a Fredholm integral equation of the first kind and can be solved by standard numerical techniques [Phillips, 1962; Tikhonov, 1963; and Twomey, 1963, 1977].

Figure 6 shows the $NO^+(v)$ VER profiles for representative days prior to and during the April 2002 and Halloween 2003 solar storms. The $NO^+(v)$ VER storm-time enhancement represents the enhancements of the E-region NO^+ and electron densities due to solar-geomagnetic forcing. The increase in the quiescent $NO^+(v)$ VER profiles below 100 km is due to a breakdown of the weak-line approximation to the limb line-of-sight radiation transfer, an assumption inherent in the Abel inversion. The $NO^+(v)$ VER profiles are representative of some of the largest enhancements observed in the SABER 4.3 um limb emission measurements during the two storm periods. The SABER data are consistent with the NOAA/POES data in sense that the Halloween 2003 storm was more intense in terms of auroral electron dosing compared to the April 2002 storm. $NO^+(v)$ VER are over a factor of two greater in the peak region and enhanced over a greater altitude region during the Halloween 2003 storm compared to the April 2002 storm. The storm-time $NO^+(v)$ VER are preliminary as the auroral electron coupling to $CO_2(\nu_3)$ through process (5) has not yet been fully assessed and implemented in the nighttime 4.3 um forward model.

A word of caution is required regarding 1-D retrievals such as the Abel inversion. The input atmospheric and external (i.e., electron precipitation) parameters responsible for the 4.3 um limb emission are highly variable in space and in time. Consequently, small-scale wave structure along the limb line-of-sight will introduce non-physical vertical structure in the derived single-profile VERs. However, it's reasonable to expect that these non-physical features in the single-profile VER retrievals will be largely filtered out in the averaging processes used to derive the storm-time corrections described in the next section.

$NO^+(v)$ VER is the key quantity used in analyzing the E-region response to solar-geomagnetic disturbances from SABER measurements of nighttime 4.3 um limb emission. The preliminary evidence suggests that the $CO_2(\nu_3)$ contribution to the measured SABER 4.3 um limb radiance can be accurately simulated and effectively removed (i.e., within ~ 20%); thus, the $NO^+(v)$ VER is an observation-based data product that is independent of any knowledge of the underlying physics and chemistry responsible for the storm-time enhancements of the major charged constituents (NO^+ ion and electron) of the ionospheric E-region, provided the electron-$CO_2(\nu_3)$ coupling via process (4) is of minor significance. As stated in the introduction, research efforts are currently underway to use the SABER-derived $NO^+(v)$ during recent solar storms to study in detail E-region ion-neutral chemistry, where large uncertainties still remain. Germane to this paper is the fact that the $NO^+(v)$ VER is also an ideal proxy to develop an empirical storm-time correction to the IRI E-region NO^+ and electron densities, for the reasons mentioned above.

6. Empirical E-region storm-time correction model

In this section we outline the approach we are developing for implementing an empirical storm-time correction to the IRI E-region NO^+ and electron densities using the SABER-derived $NO^+(v)$ VER described in the previous section.

The dynamic response of the E-region NO^+ and electron densities to solar-geomagnetic forcing is approximated using linear impulse-response theory. The numerical implementation of linear impulse-response theory using a statistical dataset is based on linear moving-average (or linear prediction) filters (Press et al., 1992). This method has been successfully applied to characterizing the response of a number of geospace parameters to external drivers (Fuller-Rowell et al., 2000; Vassiliadis et al., 2002). The main features of the our empirical impulse-response model parameterization are: (1) storm-time correction factors are derived as functions of altitude, geomagnetic latitude and longitude (or equivalently, magnetic local time), and 3-hour ap index (which is parametric in UT time), and (2) the corrections factors are determined by the ratio of the $NO^+(v)$ VER during the geomagnetically disturbed period to the quiescent $NO^+(v)$ VER (i.e., just prior to the onset of the storms).

The $NO^+(v)$ VER observations will be sorted into data bins and averaged according to altitude, geomagnetic latitude and longitude, and elapsed UT time from the onset of the storm (to correlate with the corresponding ap index). The data sorting and averaging will be done for the April 2002 and Halloween 2003 storms separately. The April 2002 storm will provide observations for the storm-time model in the southern hemisphere, while the Halloween 2003 storm will provide the observations for the northern hemisphere. The $NO^+(v)$ VER profiles within each latitude, longitude, and altitude bin will be averaged into 3-hour UT time intervals (to correspond to the 3-hour ap index). The time grid will be elapsed time starting from the onset of the storm and continuing throughout the duration of the storm. The $NO^+(v)$ VER profiles will be constructed at all longitudes and elapsed UT times using a Chebyshev polynomial fit to the binned $NO^+(v)$ VER profile data. This technique has proven successful in mapping the NOAA/POES electron energy

characteristics at all longitudes and UT times for each latitude bin. The $NO^+(v)$ VER ratios will be computed for each altitude, geomagnetic latitude and longitude, and elapsed UT time bin.

Because we are using a single activity index to characterize the E-region response at all latitudes, there may be a finite response time (lag or lead) between a change in the ap-index and the E-region response at a particular latitude and longitude. Furthermore, there may be finite a response time due to the chemical lifetime in the vertical radiative transport below 110 km, as discussed in section 4, and vertical or horizontal transport of the neutral and ion compositions, which effect the NO^+ (and electron) density as indicated in (1)-(4). The affect of a finite response time can be determined from the observational data using linear moving-average filters (or linear predictive filters) (Fuller-Rowell et at., 2000; Vassiliadis et al., 2002), as described below.

The $NO^+(v)$ VER ratios (r) at each altitude (z) and geomagnetic latitude (λ_m) and longitude (φ_m) grid point are assumed to be a linear summation of responses (F) to the solar-geomagnetic forcing (approximated by the 3-hour ap index) such that

$$r(z,\lambda_m,\varphi_m;t) = \int_{-Ts}^{T} F(z,\lambda_m,\varphi_m;\tau)\,ap(t-\tau)\,d\tau \qquad \textbf{(8)}$$

where τ is the delay time. The starting time (Ts) and the duration (T) will need to be determined by trial and error. However, the analysis of Fuller-Rowell et al. [2000] and Vassiliadis et al. [2002] offer considerable guidance. The starting time is nominally set to zero, but for numerical stability, and for the reason discussed in the paragraph above, we will initially set Ts to 5 hours. Fuller-Rowell et al. [2000] found that the foF2 ratio depended on the 33 previous hours of the ap-index. We will set our initial duration time to be 40 hours.

The impulse-response function will be determined at each altitude and geomagnetic latitude and longitude. The integral in (8) will be discretized and a linear system of equations can be defined at each altitude and geomagnetic latitude and longitude grid point using the mapped SABER measurements of the $NO^+(v)$ VER ratios at each elapsed UT time grid point throughout the storm periods. The impulse-response function (F) is calculated using a matrix inversion method based on Singular Value Decomposition (SVD) [Press et al., 1992]. The advantage of SVD is that roundoff errors in the matrix inversion are reduced compared to other methods, and the calculated impulse-response function is the best solution in the least-square sense.

We anticipate that the number of impulse-response functions needed in the model can be greatly reduced. Based on the discussion in section 4, we expect that a single impulse response function can be used at all altitudes above 110 km, and perhaps one or a small number of impulse-response functions can be used between 90 km and 110 km. Moreover, it may be adequate to use the same set of longitudinal-dependent impulse-response functions at all geomagnetic latitudes [e.g., Fuller-Rowell et al., 2000].

Once the impulse-response functions are determined, the solar-geomagnetic forcing function (or integral ap index) is defined by

$$X(z,\lambda_m,\varphi_m;t) = \int_{-Ts}^{T} F(z,\lambda_m,\varphi_m;\tau)ap(t-\tau)d\tau \quad \textbf{(9)}$$

which has the same functional form as the $NO^+(v)$ VER ratio in (8).

The empirical storm-time correction model is finally represented by

$$r(z,\lambda_m,\varphi_m;t) = \sum_{i=0}^{N} a_i(z,\lambda_m,\varphi_m)X^i(z,\lambda_m,\varphi_m;t) \quad \textbf{(10)}$$

A scatter plot of the $NO^+(v)$ VER ratios (r) versus the integral ap index (X) will determine if a non-linear fit is required (i.e., if N > 1) [Fuller-Rowell et al*.,* 2000]. The fit coefficients can be determined using all measured $NO^+(v)$ VER ratios and the SVD method for the matrix inversion, in order to minimize the residual between the measurement and the model simulation in the least-square sense [Press et al*.,* 1992].

7. Concluding remarks

The large enhancements of thermospheric infrared emission observed by the TIMED/SABER experiment during recent solar storms have fostered the development of new data products, models, and analysis tools for analyzing the response of the upper atmosphere and ionosphere to solar-geomagnetic storms. In particular, the SABER 4.3 um nighttime limb emission measurements provide a novel dataset for improving our understanding of the magnetically disturbed ionospheric E-region. The SABER-derived $NO^+(v)$ VER is an excellent proxy for characterizing the E-region response to solar-geomagnetic forcing. In this paper we summarized the current status and future plans to develop an empirical storm-time correction to the IRI E-region NO^+ and electron densities using SABER 4.3 um measurements and $NO^+(v)$ VER as an observation-based proxy. The high quality of the SABER measurements and data products, combined with the accuracy of the non-LTE and radiative transfer models, offer the potential to make significant contributions to understanding and characterizing the largely inaccessible ionospheric E-region. The storm-time correction to the IRI E-region parameterization will help quantify the effects of solar-geomagnetic disturbances on the E-region and improve the accuracy of the lower ionosphere specification for all space-based technologies that rely on radio waves propagating through the ionosphere.

Acknowledgements

CJM acknowledges helpful discussions with Geoff Crowley (SWRI) concerning the MLTI response to the April 2002 and Halloween 2003 solar storms, and Dieter Bilitza (Raytheon) concerning the IRI model. CJM also gratefully acknowledge the support of the NASA Science Mission Directorate, Sun-Earth Connection Guest Investigator

Program (now called the Heliophysics Guest Investigator Program) and the support of the Science Mission Directorate at NASA Langley Research Center.

References

Araujo-Pradere, E. A., T. J. Fuller-Rowell, and M. V. Codrescu, STORM: An empirical storm-time ionospheric correction model 1. Model description, Radio Science, 37(5), 1070, doi:10.1029/2001RS002467, 2002.

Araujo-Pradere, E. A., T. J. Fuller-Rowell, and D. Bilitza, Validation of the STORM response in IRI2000, J. Geophys. Res., 108(A3), 1120, doi:10.1029/2002JA009720, 2003.

Arfken, G., Mathematical Methods for Physicists, Third Edition, Academic Press, 1985.

Banks, P. M., C. R. Chappell, and A. F. Nagy, A new model of the interaction of auroral electrons with the atmosphere: Spectral degradation, backscatter, optical emission, and ionization, J. Geophys. Res., 79(10), 1459-1470, 1974.

Bilitza, D., International Reference Ionosphere, Radio Science, 36(2), 261-265, 2001.

Caledonia, G. E., R. E. Murphy, R. M. Nadile, and A. J. Ratkowski, Analysis of auroral infrared emission observed during the ELIAS experiment, Ann. Geophysicae, 13, 247-252, 1995.

Dothe, H., F. von Esse, and R. D. Sharma, Rotational temperatures and production mechanisms of some infrared radiators in the daylit terrestrial thermosphere, J. Geophys. Res., 101(A9), 19,715-19,721, 1996.

Duff, J. W., and D. R. Smith, The $O^+(^4S) + N_2(X^1\Sigma_g^+) \rightarrow NO^+(X^1\Sigma^+) + N(^4S)$ reaction as a source of highly rotationally excited NO^+ in the thermosphere, J. Atmos. Solar-Terr. Phys., 62, 1199-1206, 2000.

Edwards, D. P., M. Lopez-Puertas, and M. A. Lopez-Valverde, Non-LTE thermodynamic equilibrium studies of the 15-μm bands of CO_2 for atmospheric remote sensing, J. Geophys. Res., 98(D8), 14,955-14,977, 1993.

Espy, P. J., C. R. Harris, A. J. Steed, J. C. Ulwick, and R. H. Haycock, Rocketborne interferometer measurement of infrared auroral spectra, Plant. Space Sci., 36, 542, 1988.

Fox, J. L., and K. Y. Sung, Solar activity variations of the Venus thermosphere/ionosphere, J. Geophys. Res., 106(A10), 21,305-21,335, 2001.

Fuller-Rowell, T. J., E. Araujo-Pradere, and M. V. Codrescu, An empirical ionospheric storm-time correction model, Adv. Space Res., 25(1), 139-146, 2000.

Gordley, L. L., B. T. Marshall, and D. A. Chu, LINEPAK: Algorithms for modeling spectral transmittance and radiance, J. Quant. Spectrosc. Radiat. Transfer, 52(5), 563-580, 1994.

Lopez-Puertas, R. Rodrigo, A. Molina, and F. W. Taylor, A non-LTE radiative transfer model for infrared bands in the middle atmosphere. I. Theoretical basis and application to CO_2 15 μm bands, J. Atmos. Terr. Phys., 48(8), 729-748, 1986a.

Lopez-Puertas, R. Rodrigo, J. J. Lopez-Moreno, and F. W. Taylor, A non-LTE radiative transfer model for infrared bands in the middle atmosphere. II. CO_2 (2.7 and 4.3 μm) and water vapor (6.3 μm) bands and $N_2(1)$ and $O_2(1)$ vibrational levels, J. Atmos. Terr. Phys., 48(8), 749-764, 1986b.

Lopez-Puertas, M., G. Zaragoza, M. A. Lopez-Valverde, and F. W. Taylor, Non local thermodynamic equilibrium (LTE) atmospheric limb emission at 4.6 μm 1. An update of the CO_2 non-LTE radiative transfer model, J. Geophys. Res., 103(D7), 8499-8513, 1998.

Lopez-Puertas, M., M. Garcia-Comas, B. Funke, R. H. Picard, J. R. Winick, P. P. Wintersteiner, M. G. Mlynczak, C. J. Mertens, J. M. Russell III, and L. L. Gordley, Evidence for an OH(v) excitation mechanism of CO2 4.3 um nighttime emission from SABER/TIMED measurements, J. Geophys. Res., 109, D09307, doi:10.1029/2003JD004383, 2004.

Marshall, B. T., L. L. Gordley, and D. A. Chu, BANDPAK: Algorithms for modeling broadband transmission and radiance, J. Quant. Spectrosc. Radiat. Transfer, 52(5), 581-599, 1994.

McClatchey, R. A., W. S. Benedict, S. A. Clough, D. E. Burch, R. F. Calfee, K. Fox, L. S. Rothman, and J. S. Garing, AFCRL atmospheric absorption line parameters compilation, Rep. AFCRL-TR-73-0096, 78 pp., Air Force Cambridge Res. Lab., Bedford, Mass., 1973.

Mertens, C. J., M. G. Mlynczak, R. R. Garcia, and R. W. Portmann, A detailed balance of the stratospheric heat budget. 1. Radiation transfer, J. Geophys. Res., 104(D6), 6021-6038, 1999.

Mertens, C. J., M. G. Mlynczak, M. Lopez-Puertas, P. P. Wintersteiner, R. H. Picard, J. R. Winick, L. L. Gordley, and J. M. Russell III, Retrieval of mesospheric and lower thermospheric kinetic temperature from measurements of CO_2 15 μm Earth limb emission under non-LTE condition, Geophys. Res. Lett., 28(7), 1391-1394, 2001.

Mertens, C. J., M. G. Mlynczak, M. Lopez-Puertas, P. P. Wintersteiner, R. H. Picard, J. R. Winick, L. L. Gordley, and J. M. Russell III, Retrieval of kinetic temperature and carbon dioxide abundance from non-local thermodynamic equilibrium limb emission measurements made by the SABER instrument on the TIMED satellite, in Proceedings of SPIE, Remote Sensing of Clouds and the Atmosphere VII, Agia Pelagia, Crete, Greece, September 24-27, vol. 4882, 162-171, 2002.

Mertens, C. J., F. J. Schmidlin, R. A. Goldberg, E. E. Remsberg, W. D. Pesnell, J. M. Russell III, M. G. Mlynczak, M. Lopez-Puertas, P. P. Wintersteiner, R. H. Picard, J. R. Winick, and L. L. Gordley, SABER observations of mesospheric temperatures and comparisons with falling sphere measurements taken during the 2002 summer MaCWAVE campaign, Geophys. Res. Lett., 31, L03105, doi: 10.1029/2003GL018605, 2004.

Mertens et al., C. J., L. J. Cook, J. R. Winick, R. H. Picard, D. S. Evans, M. Lopez-Puertas, P. P. Wintersteiner, M. G. Mlynczak, and J. R. Russell III, and L. L. Gordley, Influence of solar-geomagnetic disturbances on SABER measurements of 4.3 um emission and the retrieval of kinetic temperature and carbon dioxide, submitted to Advances in Space Research, 2005.

Mlynczak, M. G., D. K. Zhou, and S. M. Adler-Golden, Kinetic and spectroscopic requirements for the inference of chemical heating rates and atomic hydrogen densities from OH Meinel band measurements, Geophys. Res. Lett., 25(5), 647-650, 1998.

Mlynczak, M. G., F. J. Martin-Torres, J. Russell, K. Beaumont, S. Jacobson, J. Kozyra, M. Lopez-Puertas, B. Funke, C. Mertens, L. Gordley, R. Picard, J. Winick, P.

Wintersteiner, and L. Paxton, The natural thermostat of nitric oxide emission 5.3 μm in the thermosphere observed during the solar storms of April 2002, Geophys. Res. Lett., 30(21), 2100, doi: 10.1029/2003GL017693, 2003.

Mlynczak, M. G., F. J. Martin-Torres, G. Crowley, D. P. Kratz, B. Funke, M. Lopez-Puertas, J. M. Russell III, J. Kozyra, C. Mertens, R. Sharma, L. Gordley, D. Picard, J. Winick, and L. Paxton, Energy transport in the thermosphere during the solar storms of April 2002, J. Geophys. Res., 110, A12S25, doi:10.1029/2005JA011142, 2005.

Newton, G. P., J. C. G. Walker, and P. H. E. Meijer, Vibrationally excited nitrogen in stable auroral red arcs and its effect on ionospheric recombination, J. Geophys. Res., 79(25), 3807-3818, 1974.

Phillips, B. L., A technique for the numerical solution of certain integral equations of the first kind, J. ACM, 9, 84-97, 1962.

Picard, R. H., J. R. Winick, R. D. Sharma, A. S. Zachor, P. J. Espy, and C. R. Harris, Interpretation of infrared measurements of the high-latitude thermosphere from a rocket-borne interferometer, Adv. Space Res., 7(10), 23-30, 1987.

Picone, J. M., A. E. Hedin, D. P. Drob, and A. C. Aikin, NRLMSIS-00 empirical model of the atmosphere: Statistical comparisons and scientific issues, J. Geophys. Res., 107(A12), 1468, doi:10.1029/2002JA009430, 2002.

Press, W. H., S. A. Teukolsky, W. T. Vetterling, and B. P. Flannery, Numerical Recipes in FORTRAN: The Art of Scientific Computing, Cambridge University Press, New York, 1992.

Richards, P. G., Ion and neutral density variations during ionospheric storms in September 1974: Comparison of measurement and models, J. Geophys. Res., 107(A11), 1361, doi: 10.1029/2002JA00978, 2002.

Richards, P. G., On the increase in nitric oxide density at mid latitudes during ionospheric storms, *Submitted to J. Geophys. Res.,* 2004.

Roble, R. G., Energetics of the mesosphere and thermosphere, in The Upper Mesosphere and Lower Thermosphere: A Review of Experiment and Theory, AGU Monogr. Ser., vol. 87, edited by R. M. Johnson and T. L. Killeen, American Geophysical Union, Washington DC., 1995.

Rothman, L. S., et al., The HITRAN molecular spectroscopic database: edition of 2000 including updates through 2001, J. Quant. Spectrosc. Radiat. Transfer, 82, 5-44, 2003.

Russell, J. M., III, M. G. Mlynczak, L. L. Gordley, J. Tansock, and R. Esplin, An overview of the SABER experiment and preliminary calibration results, in Proceedings of the SPIE, 44th Annual Meeting, Denver, Colorado, July 18-23, vol. 3756, pp. 277-288, 1999.

Smith, D. R., E. R. Huppi, and J. O. Wise, Observation of highly rotationally excited NO^+ emission in the thermosphere, J. Atmos. Solar-Terr. Phys., 62, 1189-1198, 2000.

Strickland, D. J., D. L. Book, T. P. Coffey, and J. A. Fedder, Transport equation techniques for the deposition of auroral electrons, J. Geophys. Res., 81(16), 2755-2764, 1976.

Tikhonov, A. N., On the solution of incorrectly stated problems and the method of regularization, Dokl. Akad. Nauk SSSR, 151, 501-504, 1963.

Torr, M. R., D. G. Torr, P. G. Richards, and S. P. Yung, Mid- and low-latitude model of thermospheric emissions 1. $O^+(^2P)$ 7320 A and $N_2(^2P)$ 3371 A, J. Geophys. Res., 95(A12), 21,147-21,168, 1990.

Twomey, S., On the numerical solution of Fredholm integral equations of the first kind by the inversion of the linear system produced by quadrature, J. Assoc. Comput., 10, 97-101, 1963.

Twomey, S., Introduction to the Mathematics of Inversion in Remote Sensing and Indirect Measurements, Elsevier, New York, 1977.

Vassiliadis, D., A. J. Klimas, S. G. Kanekal, D. N. Baker, and R. S. Weigel, Long-term-average, solar cycle, and seasonal response of magnetispheric energetic electrons to the solar wind speed, J. Geophys. Res.,107(A11), 1383, doi:10.1029/2001JA000506, 2002.

Werner, H.-J., and P. Rosmus, Ab initio calculations of radiative transition probabilities in the $X^1\Sigma^+$ ground state of the NO^+ ion, J. Molec. Spectrosc., 96, 362-367, 1982.

Winick, J. R., M. G. Mlynczak, P. P. Wintersteiner, F.-J. Martin-Torres, R. H. Picard, L. Paxton, M. Lopez-Puertas, C. J. Mertens, J. M. Russell, A. Christensen, and L. L. Gordley, Analysis of the energy input and loss in the thermosphere during the auroral events using SABER infrared limb emission and GUVI limb emission, *Proc. SPIE,* Vol. 5235, 251-263, 2004.

Winick, J. R., R. H. Picard, R. D. Sharma, R. A. Joseph, and P. P. Wintersteiner, Radiative transfer effects on aurora enhanced 4.3 micron emission, Adv. Space Res., 7(10), 17-21, 1987a.

Winick, J. R., R. H. Picard, R. A. Joseph, R. D. Sharma, and P. P. Wintersteiner, An infrared spectral radiance code for the auroral thermosphere (AARC), Rep. AFGL-TR-87-0334, Air Force Geophysical Laboratory, Hanscom Air Force Base, Massachusetts, 1987b.

Wintersteiner, P. P. R. H. Picard, R. D. Sharma, J. R. Winick, and R. A. Joseph, Line-by-line radiative excitation model for the non-equilibrium atmosphere: Application to CO_2 15 μm emission, J. Geophys. Res., 97(D16), 18,083-18,117, 1992.

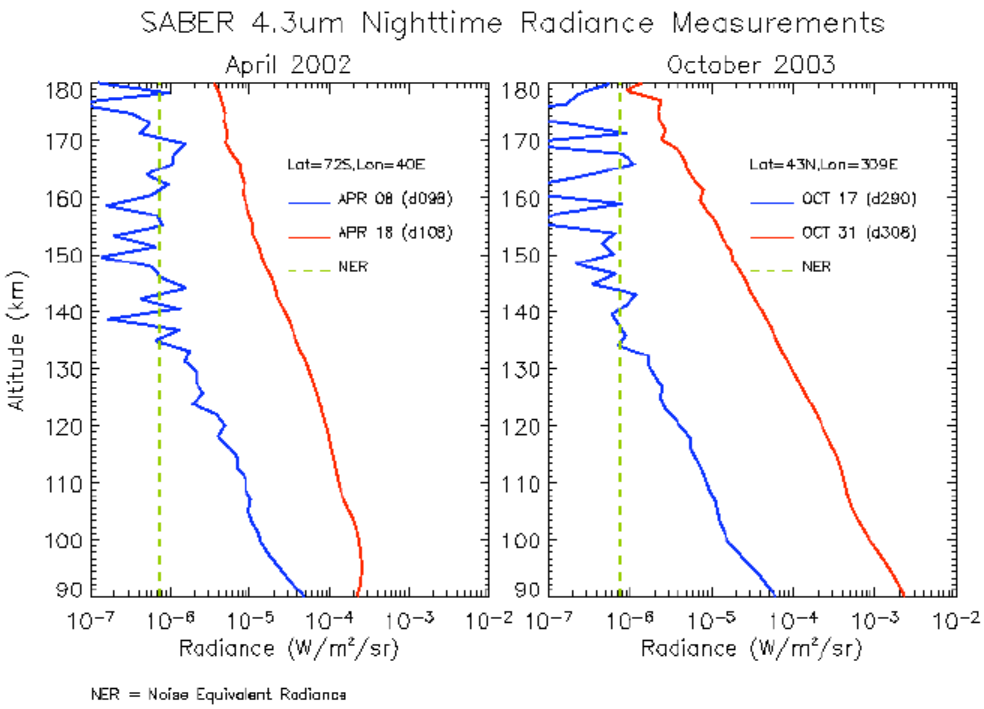

Figure 1: SABER 4.3 um limb radiance measurements during April 2002 and Halloween 2003 solar storms. The blue lines are radiances profile prior to the onset of the storms while the red lines are radiance profiles observed during the peaks of the storms. The dashed lines are the noise equivalent radiance (NER) level for the SABER 4.3 um channel.

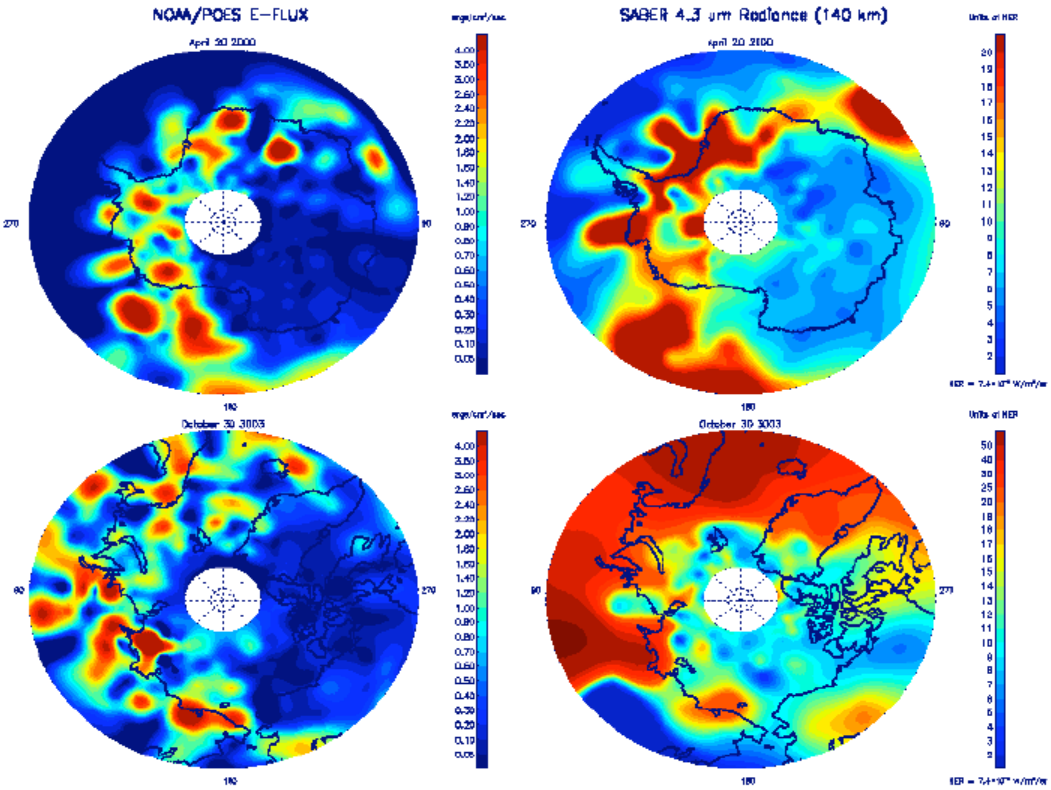

Figure 2: NOAA/POES total electron energy flux and SABER 4.3 um limb radiance measurements at 140 km for peak auroral dosing during the April 2002 and Halloween 2003 solar storms. The total electron energy flux is in units of ergs cm^{-2} s^{-1}. The SABER 4.3 um radiance measurements at 140 km are displayed in units of noise equivalent radiance (NER), which is 7.35 x 10-7 W m^2 sr^{-1}. See section 2 for further details.

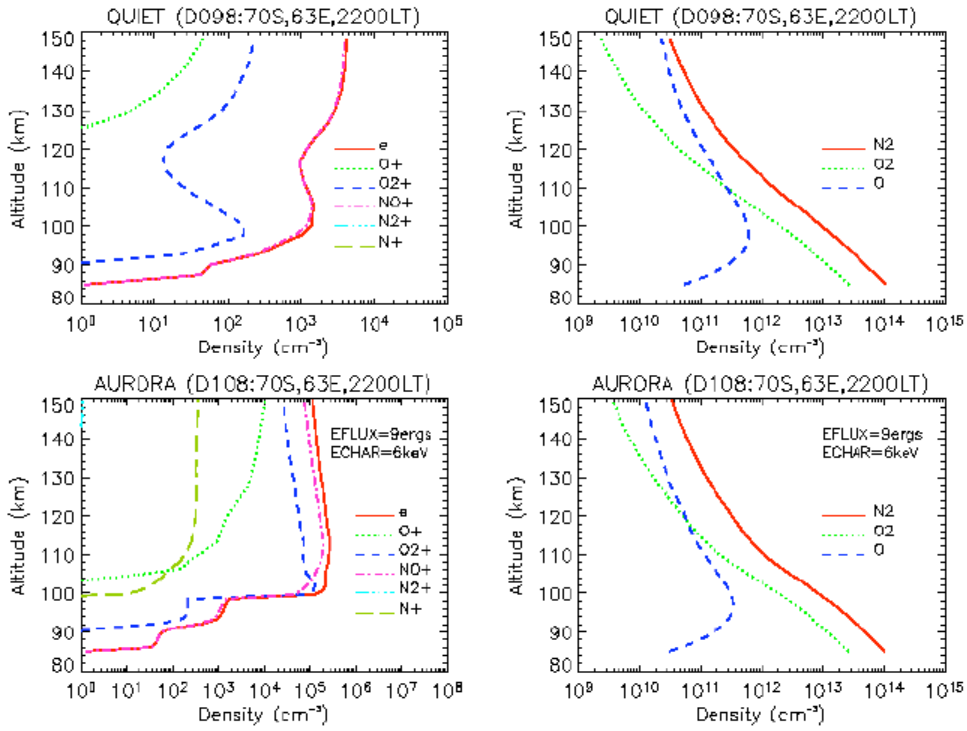

Figure 3: FLIP model simulation of ion/neutral densities for April 2002, a representative quiet day and a day of peak solar-geomagnetic activity. The electron energy characteristics used for the simulation shown in the second row is consistent with the maximum daily-averaged auroral electron dosing parameters observed by NOAA/POES on 20 April, 2002.

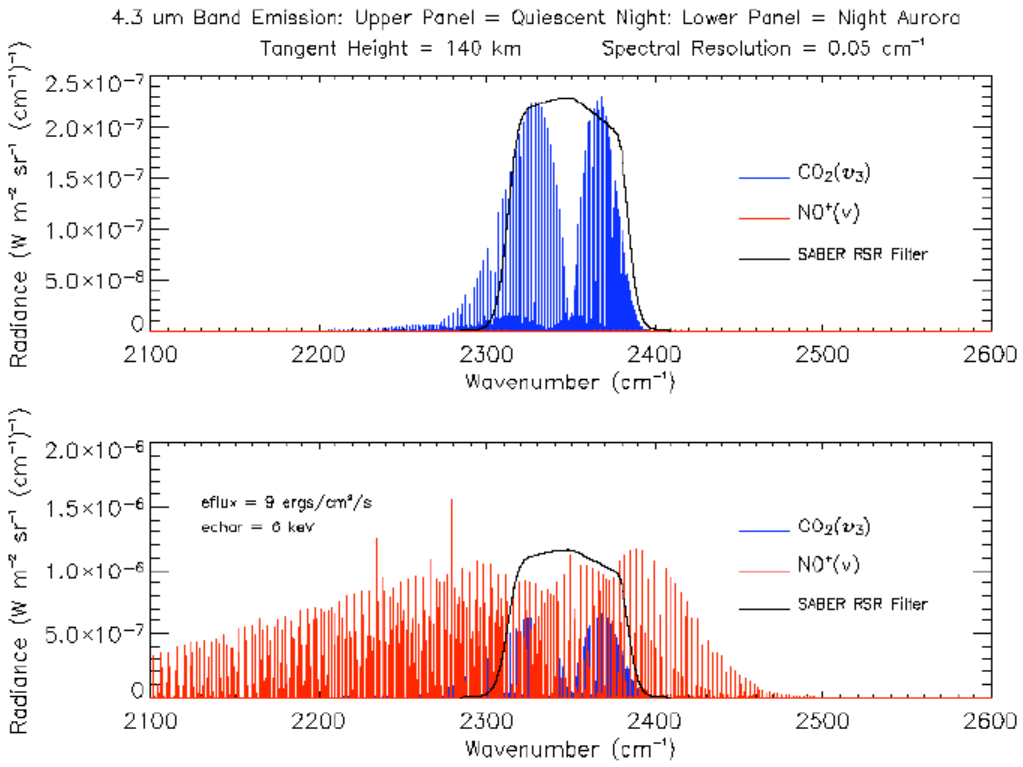

Figure 4: Simulation of 4.3 um limb emission spectra during quiescent and auroral conditions for April 2002 (same days and conditions shown in Figure 3).

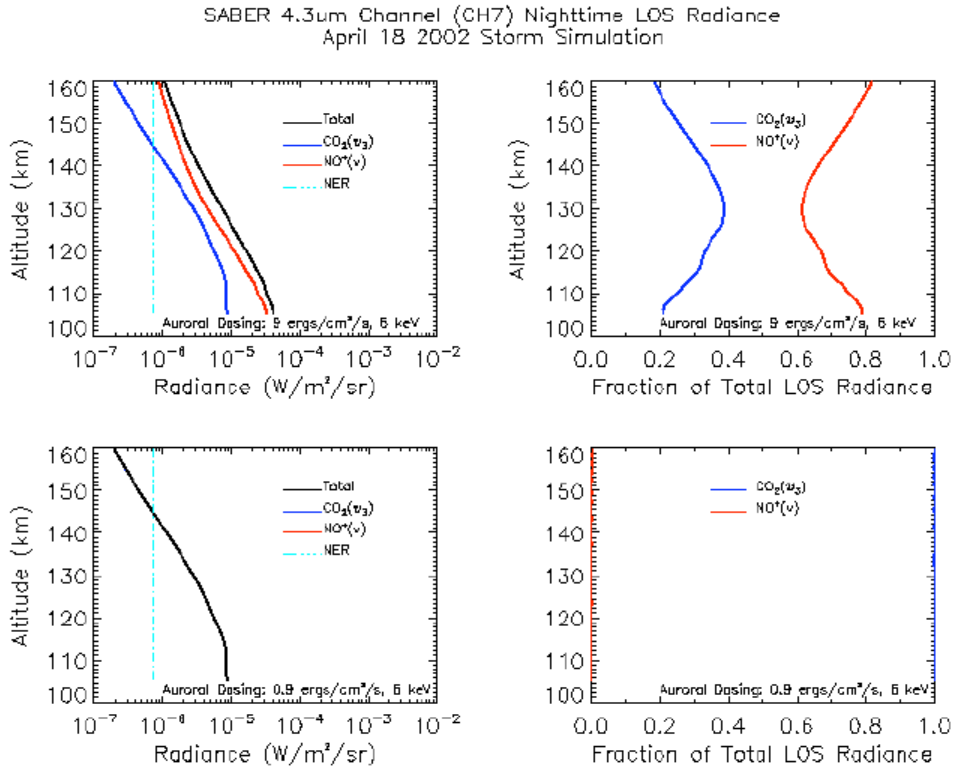

Figure 5: $NO^+(v)/CO_2(v_3)$ contribution to SABER 4.3 um channel limb emission for storm-time auroral dosing (top row) and low geomagnetic activity (bottom row). The input atmospheric data and the storm-time auroral dosing for the radiance transfer calculations correspond to the scenario shown in Figures 3 and 4. The low activity scenario was taken as one tenth the storm-time auroral dosing. The radiance profiles in this figure were obtained by convolving the radiance spectra shown in Figure 4 with the SABER 4.3 um channel spectral response function. Note, however, that Figure 4 shows the radiance spectra at one tangent altitude (i.e., at 140 km).

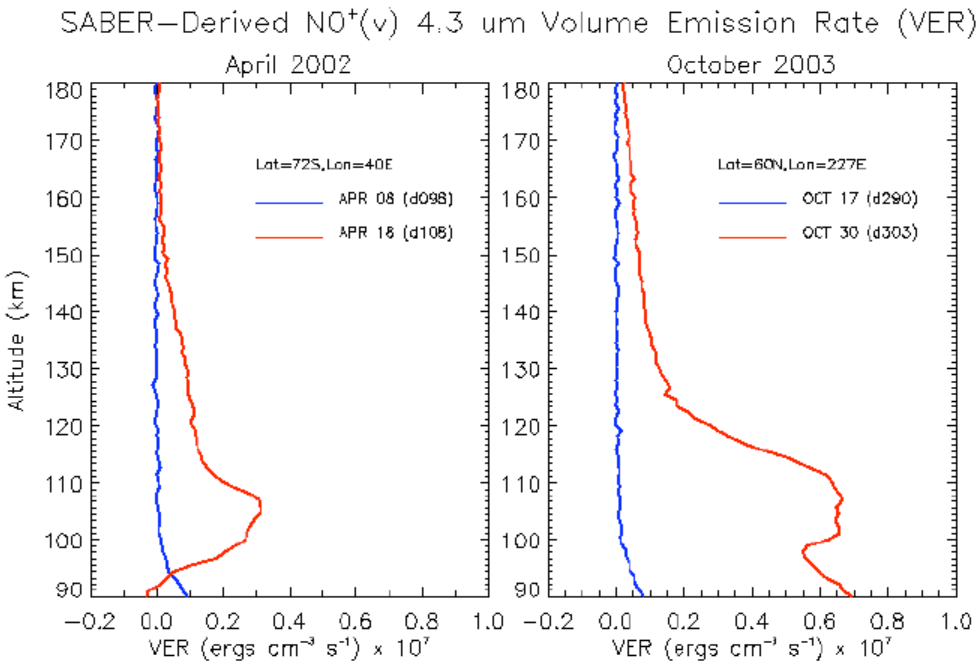

Figure 6: SABER-derived $NO^+(v)$ VER for representative days prior to and during the April 2002 and Halloween 2003 solar storms. The $NO^+(v)$ profiles were derived from the SABER 4.3 um radiance measurements shown in Figure 1.